

Selected Papers

Stationary Behavior in Effective Magnetic Moment and Magnetization of 2,3,6-Trifluorophenyl Nitronyl Nitroxide Radical Crystals

Tsuneki Kanzawa,[1] Sadafumi Nishihara,[1,2,†] Hiroyuki Nojiri,[3] and Yuko Hosokoshi*[1,2]

[1]Department of Physical Science, Graduate School of Science, Osaka Prefecture University, Sakai, Osaka 599-8531

[2]Institute for Nanofabrication Research, Osaka Prefecture University, Sakai, Osaka 599-8531

[3]Institute of Materials Research, Tohoku University, Sendai 980-8577

Received July 8, 2010; E-mail: yhoso@p.s.osakafu-u.ac.jp

A new stable organic radical, 2,3,6-trifluorophenyl nitronyl nitroxide (=2-(2,3,6-trifluorophenyl)-4,4,5,5-tetramethyl-4,5-dihydro-1*H*-imidazol-1-oxyl 3-oxide) was synthesized, and its crystal structure and magnetic properties were examined. The magnetization curve measured at 0.4 K in magnetic field up to 30 T revealed two-step saturation. A magnetization plateau was observed when the magnetization was one half the value of the saturation magnetization. The temperature dependence of the product of paramagnetic susceptibility (χ_p) and temperature (T), χ_pT ($\chi_pT \propto \mu_{eff}^2$, square of the effective magnetic moment) showed stationary behavior in the range 2–4 K at two-thirds the value at room temperature. The magnetic structure of this material could be elucidated on the basis of magnetization (M) measurements. Complementary analysis of χ_pT and M revealed the formation of magnetic clusters comprising triplet ($S = 1$) and singlet ($S = 0$) species in the ground state. The intradimer interactions were attributed to the special molecular overlaps, as reported previously. Interdimer interactions were also investigated: the difference in the molecular overlap between the trifluorophenyl groups was responsible for the difference in the sign of the magnetic coupling. This is the first experimental evidence for the molecular overlap between the phenyl groups being responsible for the strong magnetic interactions.

The magnetic properties of organic radical crystals have been studied extensively in recent decades. More than twenty organic ferromagnets have been reported since the discovery of the first organic ferromagnet, *β-p*-NPNN (Curie temperature, $T_C = 0.60$ K).[1] T_C is enhanced to 7.0 K by BBDTA·$GaCl_4$,[2] and an organic ferrimagnet[3] is also developed. Since the spins in organic radicals are isotropic in nature, networks of low dimensional antiferromagnetic spin can be used to study the effects of quantum fluctuation. Frustrated spin system such as the Kagome lattice[4] and spin-gapped systems with a magnetization plateau[5] have been developed by using organic radical crystals. Currently, there is increased focus on the use of organic radical crystals for the discovery of new magnetic phenomena. One of the characteristic in organic radicals is the *softness* and pressure effect on the magnetic properties of organic radical crystals has been reported.[6] Among them, pentafluorophenyl nitronyl nitroxide (F_5PNN) shows a peculiar magnetic behavior.[7] While this compound has a uniform chain structure at room temperature, its low-temperature magnetism is well described by the antiferromagnetic alternating chain model,[7a] and the low-energy excitation is related to the Tomonaga–Luttinger liquid.[7b] The lattice distortion occurring at temperatures below 5 K suggests the presence of strong coupling between the phonon and magnetic exchange coupling.[7c] The magnetic properties of F_5PNN are very sensitive to external pressures and are affected even by the stress coated by grease.[7d] The recent study suggests the additional exchange coupling to the chain structure, which induces incommensurate spin correlation in magnetic fields.[7e] A fluorine atom is small but rich in electrons and hence, there is very strong electrostatic repulsion between the five fluorine atoms in F_5PNN. For this reason, the molecular packing in F_5PNN is markedly different from that in other phenyl nitronyl nitroxides. To gain an insight into the magnetic interactions in F_5PNN, it is necessary to understand the relation between the molecular packing and the magnetic exchange coupling in fluorinated phenyl nitronyl nitroxide derivatives.

In this manuscript, we describe the crystal structure and magnetic properties of a new stable nitronyl nitroxide, 2-(2,3,6-trifluorophenyl)-4,4,5,5-tetramethyl-4,5-dihydro-1*H*-imidazol-1-oxyl 3-oxide (trivial name: 2,3,6-trifluorophenyl nitronyl nitroxide; abbreviation: 2,3,6-F_3PNN). We observed the stationary behavior of the product of the paramagnetic susceptibility (χ_p) and temperature (T), χ_pT ($\propto\mu_{eff}^2$, square of the effective magnetic moment) and magnetization (M). The stationary values are seemingly curious but the complementary analysis of χ_pT and M revealed the formation of magnetic clusters in this compound. We developed a magnetic model of

† Present address: Department of Chemistry, Graduate School of Science, Hiroshima University, 1-3-1 Kagamiyama, Higashi-Hiroshima 739-8526

Published on the web December 2, 2010; doi:10.1246/bcsj.20100188

2,3,6-F_3PNN on the basis of the crystal structure of this compound. While previous studies have helped in gaining a partial understanding of the molecular arrangement responsible for the magnetic exchange coupling in phenyl nitronyl nitroxide derivatives, we report for the first time importance of the overlap between the phenyl groups in the magnetic exchange coupling.

Experimental

Preparation. The 2,3,6-F_3PNN radical was synthesized by following the method described in the literatures[8] and purified by recrystallization from concentrated solutions. Single crystals were grown by slow evaporation of a concentrated solution of Et_2O–hexane. HRMS (FAB, pos) Calcd for $C_{13}H_{15}F_3N_2O_2$: $[M + H]^+$, 288.1086. Found: $m/z = 288.1057$. Anal. Calcd for $C_{13}H_{14}F_3N_2O_2$: C, 54.36; H, 4.91; N, 9.75%. Found: C, 54.46; H, 4.78; N, 9.70%.

X-ray Crystal Structure Analysis. Intensity data for structural analysis were collected using a Rigaku RAXIS Rapid diffractometer equipped with an imaging-plate detector. The frame data were processed using the Rigaku PROCESS-AUTO program,[9] and the reflection data were corrected for absorption by using the ABSCOR program.[10] The structures were solved by direct method (SHELXL-97[11]) and refined by the full-matrix least-squares techniques using the SHELXL-97[11] program. Structure refinement was carried out using anisotropic and isotropic thermal parameters for the non-hydrogen atoms and for hydrogen atoms, respectively. The positions of all the hydrogen atoms were placed at the calculated ideal positions. Crystallographic parameters are summarized in Table 1. Crystallographic data have been deposited with Cambridge Crystallographic Data Centre: Deposition numbers CCDC-791375. Copies of the data can be obtained free of charge via http://www.ccdc.cam.ac.uk/conts/retrieving.html (or from the Cambridge Crystallographic Data Centre, 12, Union Road, Cambridge, CB2 1EZ, U.K.; Fax: +44 1223 336033; e-mail: deposit@ccdc.cam.ac.uk).

Table 1. Crystallographic Data for 2,3,6-F_3PNN

Formula	$C_{13}H_{14}N_2O_2F_3$
FW	287.26
Crystal system	Triclinic
Space group	$P\bar{1}$
a/Å	10.630(6)
b/Å	11.062(5)
c/Å	13.136(8)
α/°	97.10(3)
β/°	92.45(3)
χ/°	115.94(2)
V/Å^3	1370.3(13)
Z	4
d_{calcd}/g cm^{-3}	1.392
Temperature	RT
Radiation	Mo Kα ($\lambda = 0.71075$ Å)
Unique reflections	6206
No. of reflections	4562
No. of parameters	437
R_1 ($I > 2\sigma(I)$)	0.0511
wR_2 ($I > 2\sigma(I)$)	0.1001
GOF	0.913

Magnetic Measurements. Static magnetic measurements were made using a Quantum Design MPMS superconducting quantum interference device (SQUID) magnetometer equipped with an Iquantum *i*Helium3 system: measurements were performed in the temperature (T) range 0.5–300 K and static magnetic field (B) of up to 5 T. The diamagnetic contribution was subtracted from the overall magnetization signal by using Pascal's law.

In addition, magnetization measurements were performed in pulsed magnetic fields where B was up to 30 T and $T = 0.4$ K, by using the standard inductive method; a ^{3}He cryostat was used.[12] A pulsed magnetic field with nearly sinusoidal shape was generated with a time duration of 20 ms by a 90 kJ capacitor bank. Magnetization (M) was obtained by the integration of its first derivative to time (t) dM/dt observed.

Results

Crystal Structure. The 2,3,6-F_3PNN crystals belong to a triclinic system, space group $P\bar{1}$. There are two crystallographycally independent molecules (A and B). There is no marked difference in the bond length and bond angles between the A- and B-molecules, but the dihedral angles (θ) between the best planes of the ONCNO radical moiety and the trifluorophenyl group of A- and B-molecules are different, i.e., 71 and 64°, respectively. A large θ ($\gtrsim$60°) is generally observed in the case of *o*-fluorinated phenyl nitronyl nitroxide derivatives;[5] however, θ is found to be as low as about 20° for most phenyl nitronyl nitroxide derivatives; this is because of the weak hydrogen bonding between the O atom of the NO group and the *ortho* H atom of the phenyl group.[8] Figure 1 shows the unit cell of 2,3,6-F_3PNN. The values of the short interatomic distances between the molecules are listed in Table 2. Interatomic contacts with the methyl group are omitted because their contribution to the magnetic interactions would be negligible. Polarized neutron diffraction measurements performed on the phenyl nitronyl nitroxide derivative revealed that 90% of the spin density is concentrated on the O–N–C–N–O moiety and 10% on the phenyl ring.[13] Each A- and B-molecule has the inversion symmetry and hence can form dimeric structures. The dotted and broken lines in the figure represent the shortest interatomic contact between the dimeric molecules of A and B, respectively. In the $A_{555}\cdots\bar{A}_{666}$ molecular pair, there exists a contact between the nitronyl nitroxide groups; the O(2)···O(2) distance in this case is 3.10 Å. On the other hand, in the

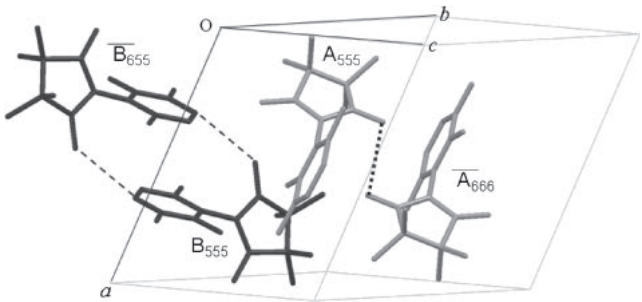

Figure 1. Crystal structure of 2,3,6-F_3PNN. Crystallographically independent molecules are labeled as A and B. Dotted and broken lines represent the shortest interatomic distances between A and B molecules, respectively.

Table 2. Short Interatomic Distances between Neighboring Molecules in 2,3,6-F_3PNN

Atom[a)] (label[b)])	Atom (label)	Distance /Å	Atom (label)	Atom (label)	Distance /Å
O(2) (A_{555})	O(2) ($\bar{A}_{666}$)	3.102	C(2) (A_{555})	O(2) ($\bar{A}_{666}$)	3.502
O(1) (A_{555})	C(5) ($\bar{B}_{655}$)	3.174	C(4) (B_{555})	C(5) ($\bar{B}_{655}$)	3.558
O(2) (B_{555})	C(4) ($\bar{B}_{655}$)	3.247	C(3) (A_{555})	C(5) ($\bar{A}_{656}$)	3.558
C(4) (A_{555})	O(1) ($\bar{A}_{656}$)	3.354	C(5) (B_{555})	C(5) ($\bar{B}_{655}$)	3.592
C(6) (B_{555})	C(4) ($\bar{B}_{655}$)	3.381	C(3) (B_{555})	C(5) ($\bar{B}_{655}$)	3.600
O(2) (A_{555})	N(2) ($\bar{A}_{666}$)	3.425			

a)

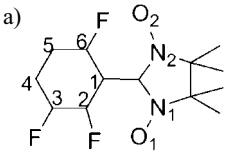

b) Symmetry operation for molecule X (X = A, B) is defined as: X_{555} (x, y, z), $\bar{X}_{666}$ ($-x+1$, $-y+1$, $-z+1$), $\bar{X}_{655}$ ($-x+1$, $-y$, $-z$), $\bar{X}_{656}$ ($-x+1$, $-y$, $-z+1$).

$B_{555}\cdots\bar{B}_{655}$ molecular pair, there are contacts between the nitronyl nitroxide and trifluorophenyl groups, and the O(2)···C(4) distance is 3.25 Å, which is doubled as a result of the inversion symmetry in B.

Figure 2 shows the molecular packing with the short interatomic contacts listed in Table 2. Figures 2a and 2b show the molecular packing involving three neighboring molecules of A and B, respectively, as viewed in the direction perpendicular to the radical plane. Although the molecular arrangement between B_{555} and $\bar{B}_{765}$ is similar to that between A_{555} and $\bar{A}_{666}$, the NO groups in the former are separated from each other. Hence the O(1)···N(1) and O(1)···O(1) distances are relatively long (3.94 and 4.04 Å, respectively). The short contact between the NO group and the phenyl group (*para* position) is also seen between A_{555} and $\bar{A}_{656}$, i.e., the C(4)···O(1) distance is 3.35 Å, similar to the case of the $B_{555}\cdots\bar{B}_{655}$ molecular pair, in which the O(2)···C(4) distance is 3.25 Å. Figures 2c and 2d show the molecular arrangements in the $A_{555}\cdots\bar{A}_{656}$ and $B_{555}\cdots\bar{B}_{655}$ molecular pairs, as viewed in the direction perpendicular to the phenyl groups, respectively. The difference in the molecular arrangements between these two molecular pairs is due to the difference in the way of molecular overlap between the phenyl groups. The *meta* C atom of A_{555} lies immediately above the one of $\bar{A}_{656}$ with the C(3)···C(5) interatomic distance being 3.56 Å. On the other hand, the *para* C atom of B_{555} lies above the *ortho* C atom of $\bar{B}_{655}$, and the C(4)···C(6) distance is 3.38 Å. Further, there is an interatomic contact between the *para* C atom and *meta* C atom, and the C(4)···C(5) distance is 3.56 Å in this case.

An interatomic contact is observed between the nitronyl nitroxide and trifluorophenyl groups of A_{555} and $\bar{B}_{655}$, i.e., O(1)···C(5), and the corresponding interatomic distance is relatively short (3.17 Å). The molecular packing is shown in Figure 2e.

Magnetic Properties. The temperature dependence of the product of paramagnetic susceptibility (χ_p) and temperature (T), χ_pT ($\chi_pT \propto \mu_{eff}^2$, square of the effective magnetic moment) is shown in Figure 3a. At room temperature, χ_pT is 0.375 emu K mol^{-1}, which agrees well with the theoretically expected value for 1 mol of magnetic species with non-interacting spin $S = 1/2$. χ_pT decreases with a decrease in T,

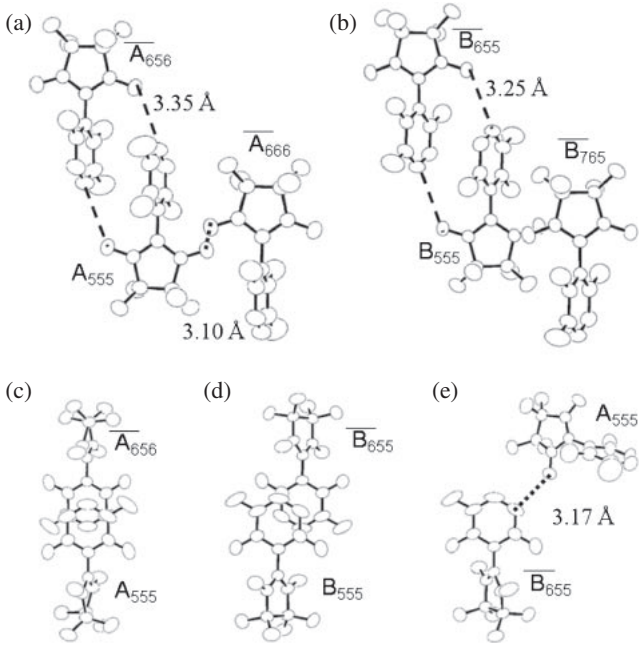

Figure 2. Molecular arrangement of neighboring molecules. Each molecule is labeled by the appropriate notation given in Table 2. (a) Three neighboring molecules of A viewed in the direction perpendicular to the O–N–C–N–O plane. (b) Three neighboring molecules of B viewed in the direction perpendicular to the O–N–C–N–O plane. (c) Molecular packing of neighboring A-molecules with contacts between the NO and phenyl groups, as viewed in the direction perpendicular to the phenyl ring. (d) Molecular packing of neighboring B-molecules having the contact between the NO and phenyl groups viewed along the direction perpendicular to the phenyl ring. (e) Neighboring molecules of A and B viewed in the direction perpendicular to the phenyl ring of B-molecule.

remains constant (0.25 emu K mol^{-1}) in the range 2–4 K, and decreases again when $T < 1$ K. The constant χ_pT value observed when $T = 2$–4 K is two-thirds the room-temperature-value.

Magnetization isotherms of 2,3,6-F_3PNN were measured by using a SQUID magnetometer for B values of up to 5 T and $T < 6$ K (inset of Figure 3). At $T = 0.5$ K and $B > 2$ T, M remain constant. The observed M value of 2800 emu mol^{-1} corresponds to one-half the full saturation value for 1 mol of $S = 1/2$. From this observation, it is evident that one-half of the molecules in 2,3,6-F_3PNN are coupled antiferromagnetically and hence remain in a non-magnetic state ($S = 0$) even at 5 T.

The stationary values observed in χ_pT and magnetization are seemingly curious. The plot of M versus B/T provides insights into the magnetic structure of 2,3,6-F_3PNN. In Figure 3b, the observed magnetization curve is compared with the theoretical curves for non-interacting spins obtained using the relation,

$$M_1 = \frac{(N_A/2)}{2S} g\mu_B S B_S(x) \quad (1)$$

where $B_s(x)$ is the Brillouin function and $x = g\mu_B SB/k_BT$. It is evident that the magnetization curves for $T < 3$ K can be well

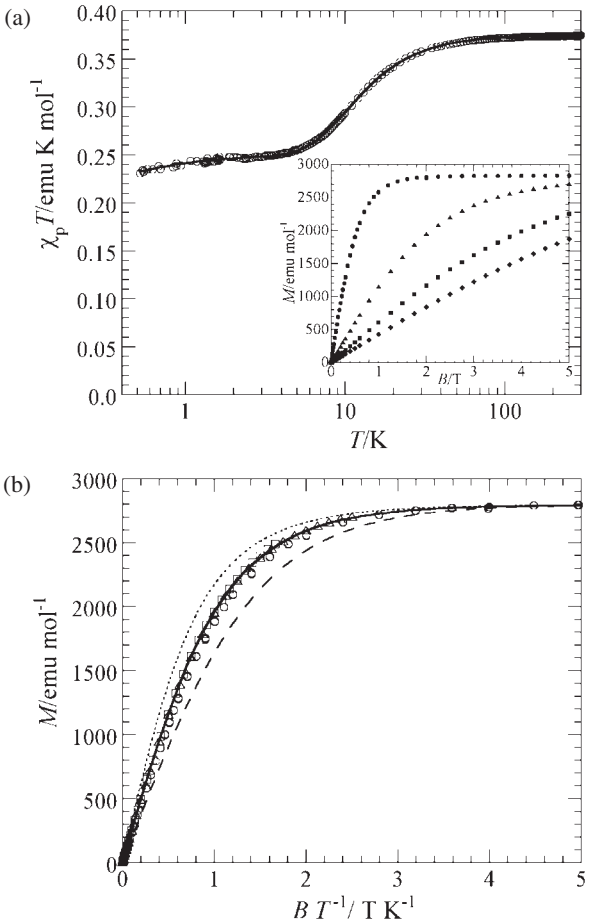

Figure 3. (a) Temperature dependence of $\chi_p T$ of 2,3,6-F_3PNN, as measured for randomly oriented crystals. The solid curve represents the calculated values (See text). Inset: Magnetization isotherms of 2,3,6-F_3PNN measured at 0.5 (●), 2 (▲), 4 (■), and 6 K (◆). (b) Magnetization (M) is plotted as a function of B/T at 0.5 (○), 2 (△), and 3 K (□). The broken, solid, and dotted curves represents the values calculated using the Brillouin function for non-interacting $S = 1/2$, $S = 1$, and $S = 3/2$, respectively.

explained by eq 1, where $S = 1$. This implies the formation of a magnetic cluster consisting of two types of spin-pairs (dimers). One of the spin-pairs is in the triplet state ($S_1 = 1$) and the other is in the singlet state ($S_2 = 0$); the former and latter spin-pairs are formed by the ferromagnetic and antiferromagnetic coupling between two $S = 1/2$ spins, respectively. If this magnetic cluster is formed, χ_p should obey Curie's law ($\chi_p = C/T$); the Curie constant C is given by

$$C = \sum_{i=1}^{2} \frac{(N_A/4)g^2{\mu_B}^2 S_i(S_i+1)}{3k_B} \tag{2}$$

where $S_1 = 1$ and $S_2 = 0$. The calculated value of C (=0.25 emu K mol^{-1}) agrees well with the observed $\chi_p T$ value when T is in the range 2–4 K. The magnetic model that can explain both of the stationary values in $\chi_p T$ and M in the aforementioned range is elucidated in Figure 4a. A schematic of the spin alignment at low T is shown in Figure 4b. From this figure, the formation of 1/4 mol of two types of magnetic

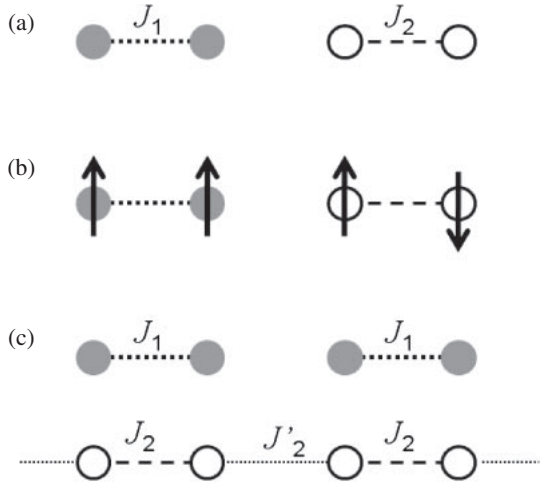

Figure 4. Magnetic model of 2,3,6-F_3PNN. (a) Model showing two independent dimers corresponding to Hamiltonian (3). (b) Schematic illustration of spin alignment at low temperatures in the model (a), with $J_1 > 0$ and $J_2 < 0$. (c) Modified model with interdimer exchange coupling J_2' between dimer-2 is taken into account. The symmetry of the crystal structure suggests the alternating chain model. Hamiltonian of this magnetic model is written by eq 7.

species, one with $S_1 = 1$ and the other with $S_2 = 0$, is evident. In fact, the crystal structure analysis reveals two types of dimeric structures. Now, we analyze the behavior of $\chi_p T$ and M over the entire range of T and B considered in this study, by using the model shown in Figure 4a. The Hamiltonian is given by

$$H = -2J_1 \sum_{i=1}^{(N_A/2)-1} \boldsymbol{S}_{2i} \cdot \boldsymbol{S}_{2i+1} - 2J_2 \sum_{i=N_A/2}^{N_A-1} \boldsymbol{S}_{2i} \cdot \boldsymbol{S}_{2i+1} \tag{3}$$

We assign positive and negative signs of J_1 and J_2, which are responsible for the formation of $S_1 = 1$ and $S_2 = 0$ species in the ground state, respectively. The spin pair for the former case is called as dimer-1 and that for the latter case is called dimer-2. The temperature dependence of the susceptibility is described by the contributions of both dimer-1 and dimer-2, each of which is represented by the formula,

$$\chi_i = \frac{(N_A/2)g^2{\mu_B}^2}{k_B T} \frac{1}{3 + \exp(-2J_i/k_B T)} \quad (i = 1, 2) \tag{4}$$

The slight decrease in $\chi_p T$ observed at $T \leq 2$ K suggests the existence of weak interdimer interactions. In this temperature regime, χ_2 becomes zero because of the formation of $S_2 = 0$ and hence, we introduce the weak interdimer interactions by the mean-field approximation as follows:

$$\chi_p = \frac{\chi_1}{1 - \lambda\chi_1} + \chi_2 \tag{5}$$

where λ is the mean-field coefficient and is related to the interdimer exchange coupling (J_1') between dimer-1 and the number of nearest neighbors (z):

$$\lambda = \frac{2zJ_1'}{(N_A/2)g^2{\mu_B}^2} \tag{6}$$

By least square fitting procedure, we obtain the parameter sets $2J_1/k_B = 16.3 \pm 0.7$ K, $2J_2/k_B = -22.8 \pm 0.3$ K, and $2zJ_1'/k_B = -0.131 \pm 0.005$ K, which are well consistent with the data observed for the entire range of T considered in this study, as shown by the solid curve in Figure 3a.

The possibility of the existence of the interdimer interactions (J_2') between dimer-2 is also examined. The symmetry of the crystal structure suggests that dimer-2 is coupled each other to form an alternating chain as is shown in Figure 4c. The Hamiltonian is given by

$$H = -2J_1 \sum_{i=1}^{(N_A/2)-1} \boldsymbol{S}_{2i} \cdot \boldsymbol{S}_{2i+1} - \sum_{i=N_A/2}^{N_A-1} \{2J_2 \boldsymbol{S}_{2i} \cdot \boldsymbol{S}_{2i+1} + 2J_2' \boldsymbol{S}_{2i+1} \cdot \boldsymbol{S}_{2i+2}\} \quad (7)$$

We examined the cases for $J_2' > 0$ and $J_2' < 0$, where χ_2 (in eq 5) indicates the magnetic susceptibility in (1) the alternating chain model with ferromagnetic and antiferromagnetc interactions[14] and (2) the antiferromagnetic alternating chain model,[15] respectively. After the least-squares fitting for $J_2' > 0$, we obtaine the parameter sets $2J_1/k_B = 15.0 \pm 0.9$ K, $2J_2/k_B = -22.3 \pm 0.2$ K, $\alpha_2 = J_2'/J_2 = 0.0 \pm 0.02$, and $2zJ_1'/k_B = -0.138 \pm 0.004$ K. The estimated value of $J_2' = 0$, indicating that this model is reduced to Hamiltonian (3) and that the slight difference between the obtained parameters results from the limitation of the polynomial expression. In the case of $J_2' < 0$, least-squares-fitting yields the parameter sets $2J_1/k_B = 21.4 \pm 0.9$ K, $2J_2/k_B = -24.0 \pm 0.1$ K, $\alpha_2 = J_2'/J_2 = 0.14 \pm 0.02$, and $2zJ_1'/k_B = -0.143 \pm 0.004$ K. The curve plotted using the calculated parameters is identical to that obtained for the model based on eq 3, which is shown by the solid curve in Figure 3a. Thus, we conclude that the interdimer interactions between dimer-2 should be in the range $0 \geq 2J_2'/k_B \geq -3.4$ K.

The validity of this magnetic model is confirmed by analyzing the magnetization curves shown in Figure 5. Figure 5a shows the B/T dependence of M in the low-field region. The slope in this case is slightly different from the theoretical curve obtained on the basis of the Brillouin function for $S = 1$. Below 2 K, the slope decreases with a decrease in T, whereas above 4 K, the slope increases with an increase in T. The former phenomenon is attributed to the effect of the weak antiferromagnetic interdimer interactions between dimer-1, while the latter is due to the thermal population of the excited state in dimer-2. We first study the magnetization behavior below 2 K. The M value of the weakly coupled $S = 1$ species is calculated by using the mean-field approximation. For calculating the Brillouin function, we use effective field $B + \lambda M$ instead of the applied field B. The values calculated using the above parameter $2zJ_1'/k_B = -0.13$ K are plotted in Figure 5a (solid curves); the calculated values are in good agreement with the observed data at 0.5 and 2 K. Next, we discuss the data observed at $T \geq 4$ K. The energy gap (Δ) between the ground state ($S = 0$) and excited state ($S = 1$) of dimer-2 is expected to be $\Delta = 2|J_2|/k_B = 22.8$ K. Although dimer-2 is in the nonmagnetic ground state, nonzero magnetization is expected at $T \geq 4$ K; this is because of the thermal excitation of dimer-2 to the excited $S = 1$ state even B is less than 5 T. The magnet-

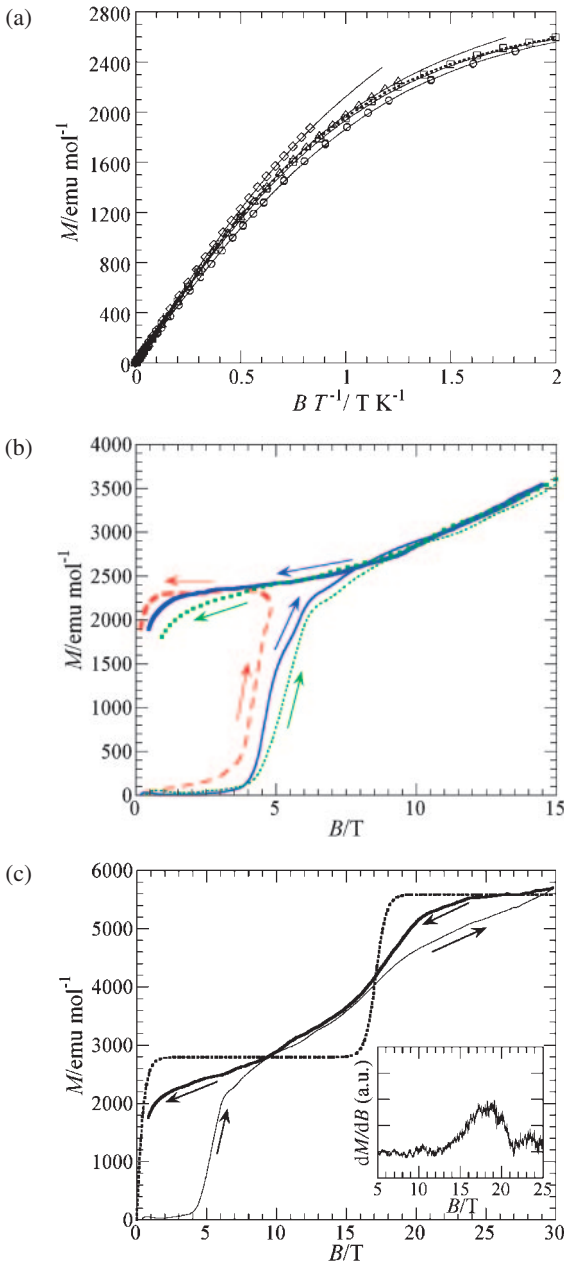

Figure 5. (a) Plot of magnetization (M) versus B/T in the low-field region. Data measured at 0.5 (○), 2 (□), 4 (△) and 6 K (◇) are compared with the calculated values represented by solid curves (See text). (b) Magnetization curves measured at 0.4 K in a pulsed magnetic field. The broken, solid, and dotted curves represent the data obtained at the magnetic fields of up to 4, 15, and 30 T, respectively. Thin and thick curves correspond to the up and down sweeps, respectively. Arrows indicate sweep directions. (c) Whole magnetization curve at 0.4 K. Solid curves are the data obtained in a pulsed magnetic field up to 30 T and thin and thick curves correspond to the up and down sweeps, respectively. Arrows indicate sweep directions. Dotted curve show the calculated values obtained using Hamiltonian (3). The combination of the Brillouin function of $S = 1$ and the dimer model with intradimer exchange coupling of $2J_2/k_B = -23$ K is used. Inset: Differential magnetization curve in the down sweep measured at 0.4 K.

ization isotherm for the isolated dimers in which two $S = 1/2$ spins are coupled (J_i) is calculated by using the following equation:

$$M_i = \frac{N_A}{2} g\mu_B \frac{\exp(y) - \exp(-y)}{1 + \exp(-2J_i/k_BT) + \exp(y) - \exp(-y)} \quad (8)$$

where

$$y = \frac{g\mu_B B}{k_B T} \quad (9)$$

The combined contributions of dimer-1 (mentioned above) and dimer-2, which is obtained by substituting $2J_2/k_B = -23$ K in eq 8, are shown by the solid curves in Figure 5a; the calculated data fit the observed data at 4 and 6 K well.

Finally, we describe the magnetization curve measured for B values of up to 30 T, which are achieved by using a pulsed magnet at $T = 0.4$ K. The results are shown in Figures 5b and 5c. A large hysteresis is observed between the up and down sweeps of the magnetic field. The low-field data in the different runs up to 4, 15, and 30 T are shown in Figure 5b. Below 4 T, The effective magnetization does not occur during rapid sweeping in the up scan, suggesting that the relaxation time is longer than the sweeping period. In other words, thermal relaxation is quenched by the fast sweeping pulsed field, which allows us to observe the nonequilibrium behavior of M. This effect is well pronounced in the case of the spin system with weak coupling between the magnetic clusters.[12] In 2,3,6-F_3PNN, the competition between thermal relaxation and fast changes in B is thought to be the reason for M being smaller than that at equilibrium in the low-field region, even during the down sweep; this suggests that the magnetic coupling between dimer-1 ($S = 1$) is very weak.

Above 10 T, magnetization gradually increases and reaches full saturation value for 1 mol of $S = 1/2$ when B exceeds 20 T. The appearance of this step is evidence for the antiferromagnetic exchange coupling (J_2) in the dimer-2. Figure 5c shows the comparison of the observed data and the calculated data. The dotted curve represents the values calculated based on the model of eq 3. The second step observed at 17 T also shows hysteresis between the up and down sweeps. This is not due to magnetic anisotropy because this compound is a highly isotropic spin system and the anisotropy of the g-factor determined by the electron spin resonance at room temperature is less than 0.5%. It is certain that interdimer interactions may cause a broader step in magnetization curve but that cannot yield such hysteresis. As an origin of the hysteresis, it is notable that because of the so-called magnetocaloric effect, the effective temperature of the spin system may differ from the bath temperature in fast-sweeping pulsed magnetic fields. This effect is also pronounced in spin systems where the magnetic clusters are weakly coupled. The slower saturation observed than that calculated may partly reflect the nonequilibrium behavior of M. Nevertheless we can estimate the energy separation between the ground and excited states in dimer-2. For a clearer representation of the second step, we have provided the derivative curve of M versus B in the inset of Figure 5c. The maximum slope of the dM/dB curve is observed at the crossing point (B_c) of the energy levels of the ground state ($S = 0$) and the excited state ($S = 1$) in dimer-2. The energy gap (Δ) between the energy levels is given by

$$\Delta = 2|J_2| = g\mu_B B_c \quad (10)$$

The derivative curve of dM/dB shows a peak at $B_c = 17.5$ T, and the exchange coupling calculated using eq 10 is $2J_2/k_B = -23.5$ K, which is consistent with that estimated from the χ_pT analysis ($2J_2/k_B = -22.8 \pm 0.3$ K). Complementary analysis of χ_pT and M helps in the accurate elucidation of the magnetic model; the exchange coupling estimated from the magnetization curve at low temperature is always slightly greater than that from temperature dependence of the susceptibility.[5] This difference is probably due to the lattice contraction at low T. It is noteworthy that interdimer interactions may be responsible for the broadening of the second step. The interdimer interaction between dimer-2 is estimated to be at most -3.4 K (alternating ratio, $\alpha = J_2'/J_2 = 0.14$) by the analysis of χ_pT. The theoretical magnetization curve for $T = 0$ predicts a 30% broadening of the saturation at around B_c when $\alpha = 0.2$,[16] which is consistent with the observations.

Discussion

In this section, we focus on the interrelation between the magnetic model and the crystal structure. The stationary behavior means the formation of magnetic clusters. The saturation ratio of the magnetization versus magnetic fields demonstrates the formation of $S = 1$ species. The constant value of M in the range 2–5 T indicates the alignment of only 1/2 mol of the $S = 1/2$ species. Thus, 50% of the molecules in a unit cell undergo magnetization, and the rest are in nonmagnetic state owing to the strong antiferromagnetic coupling. This antiferromagnetic coupling is destroyed when $B_c = 17.5$ T, and full saturation is realized above 20 T. Magnetization measurements reveal the formation of 1/4 mol of $S = 1$ species by the ferromagnetic coupling between 1/2 mol of the $S = 1/2$ species and the formation of 1/4 mol of $S = 0$ species by the antiferromagnetic coupling between 1/2 mol of the $S = 1/2$. This magnetic model explains the stationary values of M and χ_pT. By taking the symmetry in the crystal structure into account, we state that molecules A and B are responsible for the formation of dimer-1, in which $S = 1$ in the ground state, and dimer-2, in which $S = 0$ in the ground state, or vice versa. The results of magnetic measurements suggest that the magnetic interactions between the molecules A and B are considerably weaker rather than the intradimer interactions of dimer-1 and dimer-2. This implies that the second shortest interatomic distance between A_{555} and $\bar{B}_{655}$ (shown in Figure 2e) does not make any significant contribution to the magnetic coupling. The reason for this can be understood by considering the molecular overlap between the π-orbitals of these molecules. The side-by-side contact between the molecules results in smaller degree of overlap than that in the case of π–π stacking. Hence, dimer-2, in which two $S = 1/2$ spins are coupled antiferromagnetically ($2J_2/k_B = -23$ K) can be assigned to the $A_{555}\cdots\bar{A}_{666}$ molecular pair, which has the shortest interatomic distance (O(2)···O(2)) 3.10 Å. The intermolecular contact between the NO groups, on which most of the spin density is concentrated, always yields antiferromagnetic coupling. The magnitude of the antiferromagnetic

interactions in this case is consistent with previously reported values: $2J/k_B = -20$ K for N···O (3.71 Å) in 4-trifluoromethylphenyl nitronyl nitroxide.[17] Dimer-1, in which two $S = 1/2$ spins are coupled ferromagnetically ($2J_1/k_B = 16$ K), is assigned to the B_{555}···$\bar{B}_{655}$ molecular pair, which has the third shortest contact (O(2)···C(4)), with the interatomic distance being 3.25 Å. Ferromagnetic coupling is often observed in intermolecular arrangements that involve contacts between the NO and phenyl groups. In (*m*-MPYNN)·$(BF_4)_{0.72}$·$I_{0.28}$·$(H_2O)_{0.17}$, where *m*-MPYNN is *m*-methylpyridinium nitronyl nitroxide, ferromagnetic coupling ($2J/k_B = 22.6$ K) has been reported for O···C (3.00 Å) and O···N (3.19 Å).[4]

Next, we consider the weak interdimer interactions between dimer-1. Analysis of the χ_pT and M reveals a weak interdimer exchange coupling ($2zJ_1'/k_B = -0.13$ K). Since dimer-1 has been identified to be the B_{555}···$\bar{B}_{655}$ molecular pair, as described above, we can find the interdimer contact in Figure 2b. Interatomic contacts between the NO groups (O(1)···N(1) (3.94 Å) and O(1)···O(1) (4.04 Å)) in B_{555} and $\bar{B}_{765}$ are relatively long. The exchange coupling ($2J_1'/k_B = -0.07$ K) obtained when assuming $z = 2$ is attributable to the magnetic interactions between B_{555} and $\bar{B}_{765}$. The exact magnetic model for B-molecules should be an alternating chain according to the crystal structure, but the estimated alternating ratio is so small ($\alpha_1 = J_1'/J_1 = -0.004$) that no analytical calculation is available[14] and the mean-field approximation is appreciable.

Finally, we discuss the interdimer interactions between dimer-2. As mentioned above, dimer-2 is identified to the A_{555}···$\bar{A}_{666}$ molecular pair and the interdimer exchange coupling ($0 \geq 2J_2'/k_B \geq -3.4$ K) is attributable to the contacts between A_{555}···$\bar{A}_{656}$. As is seen in Figure 2a, the short contact between the NO and phenyl groups is remarkable in A_{555}···$\bar{A}_{656}$; the C(4)···O(1) distance is 3.35 Å. This type of molecular contact is seen in the B_{555}···$\bar{B}_{655}$ molecular pair which is responsible for the ferromagnetic exchange coupling ($2J_1/k_B = 16$ K) as dimer-1; the O(2)···C(4) distance is 3.25 Å between the NO and phenyl groups. The difference in the sign of the magnetic coupling between the A_{555}···$\bar{A}_{656}$ and B_{555}···$\bar{B}_{655}$ molecular pair cannot be explained on the basis of the shortest interatomic contact alone, since each molecular pair has a shortest contact between the NO group and C(4) of the phenyl group (*para* position). The above-mentioned difference is attributed to the difference in the molecular packing of the trifluorophenyl groups between A_{555}···$\bar{A}_{656}$ and B_{555}···$\bar{B}_{655}$. As described in previous section of crystal structure, the *meta* C atom of A_{555} lies immediately above the one of $\bar{A}_{656}$ (Figure 2c), whereas the *para* C atom of B_{555} lies above the *ortho* C atom of $\bar{B}_{655}$ (Figure 2d). The molecular overlap between the trifluorophenyl groups in A_{555}···$\bar{A}_{656}$ may lead to antiferromagnetic interactions which surpasses the contribution of the ferromagnetic interactions resulting from the O(1)···C(4) contact (contact between the NO and phenyl groups). As a result, the antiferromagnetic coupling in the A_{555}···$\bar{A}_{656}$ molecular pair is in the range $0 \geq 2J_2'/k_B \geq -3.4$ K. We cannot judge the sign of the magnetic interactions resulting from the molecular overlap between the trifluorophenyl groups in B_{555}···$\bar{B}_{655}$. The ferromagnetic coupling ($2J_1/k_B = 21$ K) in B_{555}···$\bar{B}_{655}$ is mainly due to the ferromagnetic contribution by the C(4)···O(2) contact (contact between the NO and phenyl groups). This is the first experimental evidence of the significant role played by the molecular overlap between the phenyl groups in magnetic exchange coupling. The present results may shed light on the interchain magnetic coupling in the crystals of F_5PNN.[7] There are experimental and theoretical reports on the change in the sign of the magnetic coupling caused by the replacement of a hydrogen atom on the phenyl ring with a halogen atom.[18] Further experimental and theoretical studies must be carried out on series compounds of fluorinated phenyl nitronyl nitroxide to elucidate the magneto–structural correlation in the case of phenyl groups. We have been examining the crystal structure and magnetic properties of a series of fluorinated phenyl nitronyl nitroxide derivatives in order to clarify the molecular packing that is responsible for the magnetic coupling in these compounds.

Conclusion

The crystal structure and magnetic properties of a new organic radical 2,3,6-F_3PNN have been investigated. A peculiar phenomenon observed in the case of this radical is the stationary behavior in M and χ_pT in a given temperature range. Complementary analysis of χ_pT and M reveal the formation of magnetic clusters in this compound. Analysis of the magnetization curve is an efficient method of elucidating the magnetic model. In the ground state, two different species with $S = 1$ and $S = 0$ are formed, where two $S = 1/2$ spins are coupled ($2J_1/k_B = 16$ K and $2J_2/k_B = -23$ K, respectively). These two exchange couplings are attributed to the formation of special molecular pairs in which there are contacts between the NO groups and trifluorophenyl groups or between the NO groups, respectively. The 2,3,6-F_3PNN crystals also show another molecular pair in which there are the contacts between the NO and trifluorophenyl groups: the exchange coupling in this case is $0 \geq 2J_2'/k_B \geq -3.4$ K, as decided from the analysis of the magnetic properties. The difference in the sign of the magnetic exchange coupling between J_1 and J_2' is attributed to the difference in the molecular packing of the trifluorophenyl groups. This is the first evidence for the important role played by the relative arrangement of the phenyl groups among phenyl nitronyl nitroxide derivatives in the observed magnetic interactions.

High-field magnetization measurements in pulsed magnetic field were performed under the interuniversity cooperative research program of the Institute for Materials Research, Tohoku University. The authors acknowledge Mr. G. Tanaka's assistance in the magnetization measurements performed in the pulsed magnetic field. This study was partially supported by Kakenhi No. 21605010 and by the Asahi Glass Foundation. HN acknowledges Kakenhi No. 20244052.

References

1 a) M. Tamura, Y. Nakazawa, D. Shiomi, K. Nozawa, Y. Hosokoshi, M. Ishikawa, M. Takahashi, M. Kinoshita, *Chem. Phys. Lett.* **1991**, *186*, 401. b) Y. Nakazawa, M. Tamura, N. Shirakawa, D. Shiomi, M. Takahashi, M. Kinoshita, M. Ishikawa, *Phys. Rev. B* **1992**, *46*, 8906.

2 W. Fujita, K. Awaga, *Chem. Phys. Lett.* **2004**, *388*, 186.

3 Y. Hosokoshi, K. Katoh, Y. Nakazawa, H. Nakano, K.

Inoue, *J. Am. Chem. Soc.* **2001**, *123*, 7921.

4 a) K. Awaga, T. Okuno, A. Yamaguchi, M. Hasegawa, T. Inabe, Y. Maruyama, N. Wada, *Phys. Rev. B* **1994**, *49*, 3975. b) K. Awaga, T. Inabe, T. Nakamura, M. Matsumoto, Y. Maruyama, *Mol. Cryst. Liq. Cryst.* **1993**, *232*, 69.

5 Y. Hosokoshi, Y. Nakazawa, K. Inoue, K. Takizawa, H. Nakano, M. Takahashi, T. Goto, *Phys. Rev. B* **1999**, *60*, 12924.

6 K. Takeda, M. Mito, in *The Magnetism of π-Orbitals under Pressure* in *Carbon-Based Magnetism: An Overview of the Magnetism of Metal Free Carbon-Based Compounds and Materials*, ed. by T. Makarova, F. Palacio, Elsevier B. V., **2005**, pp. 131–158.

7 a) M. Takahashi, Y. Hosokoshi, H. Nakano, T. Goto, M. Takahashi, M. Kinoshita, *Mol. Cryst. Liq. Cryst.* **1997**, *306*, 111. b) Y. Yoshida, N. Tateiwa, M. Mito, T. Kawae, K. Takeda, Y. Hosokoshi, K. Inoue, *Phys. Rev. Lett.* **2005**, *94*, 037203. c) T. Matsushita, Y. Kugimiya, K. Shimizu, N. Wada, Y. Yoshida, T. Kawae, K. Takeda, Y. Hosokoshi, K. Inoue, Proceedings of the 24th International Conference on Low Temperature Physics, AIP Conference Proceedings, **2006**, Vol. 850, p. 1029. d) M. Mito, T. Kawae, Y. Hosokoshi, K. Inoue, M. Kinoshita, K. Takeda, *Solid State Commun.* **1999**, *111*, 607. e) Y. Yoshida, T. Kawae, Y. Hosokoshi, K. Inoue, N. Maeshima, K. Okunishi, K. Okamoto, T. Sakai, *J. Phys. Soc. Jpn.* **2009**, *78*, 074716.

8 Y. Hosokoshi, M. Tamura, M. Kinoshita, H. Sawa, R. Kato, Y. Fujiwara, Y. Ueda, *J. Mater. Chem.* **1994**, *4*, 1219.

9 *PROCESS-AUTO, Automatic Data Acquisition and Processing Package for Imaging Plate Diffractometer*, Rigaku Corporation, Tokyo, Japan, **1998**.

10 T. Higashi, *ABSCOR, Empirical Absorption Correction based on Fourier Series Approximation*, Rigaku Corporation, Tokyo, Japan, **1995**.

11 G. M. Sheldrick, *SHELX97, Program for Crystal Structure Determination*, University of Göttingen, Göttingen, Germany, **1997**.

12 a) H. Nojiri, K.-Y. Choi, N. Kitamura, *J. Magn. Magn. Mater.* **2007**, *310*, 1468. b) T. Yamase, E. Ishikawa, K. Fukaya, H. Nojiri, T. Taniguchi, T. Atake, *Inorg. Chem.* **2004**, *43*, 8150.

13 a) A. Zheludev, V. Barone, M. Bonnet, B. Delley, A. Grand, E. Ressouche, P. Rey, R. Subra, J. Schweizer, *J. Am. Chem. Soc.* **1994**, *116*, 2019. b) A. Zheludev, E. Ressouche, J. Schweizer, P. Turek, M. Wan, H. Wang, *J. Magn. Magn. Mater.* **1995**, *140–141*, 1441.

14 J. J. Borras-Almenar, E. Coronado, J. Curely, R. Georges, J. C. Gianduzzo, *Inorg. Chem.* **1994**, *33*, 5171.

15 J. W. Hall, W. E. Marsh, R. R. Weller, W. E. Hatfield, *Inorg. Chem.* **1981**, *20*, 1033.

16 J. C. Bonner, S. A. Friedberg, H. Kobayashi, D. L. Meier, H. W. Blöte, *Phys. Rev. B* **1983**, *27*, 248.

17 K. Nozawa, Y. Hosokoshi, D. Shiomi, M. Tamura, N. Iwasawa, H. Sawa, R. Kato, M. Kinoshita, *Synth. Met.* **1993**, *56*, 3323.

18 a) J. Cirujeda, E. Hernàndez-gasió, F. L. de Panthou, J. Laugier, M. Mas, E. Molins, C. Rovira, J. J. Novoa, P. Rey, J. Veciana, *Mol. Cryst. Liq. Cryst.* **1995**, *271*, 1. b) Y. Hosokoshi, M. Tamura, K. Nozawa, S. Suzuki, H. Sawa, R. Kato, M. Kinoshita, *Mol. Cryst. Liq. Cryst.* **1995**, *271*, 115. c) Y. Hosokoshi, M. Takahashi, T. Goto, K. Inoue, *J. Magn. Magn. Mater.* **1998**, *177–181*, 713.